J Comp Physiol A (2012) 198:567–582
DOI 10.1007/s00359-012-0730-5

ORIGINAL PAPER

Centrally patterned rhythmic activity integrated by a peripheral circuit linking multiple oscillators

John Jellies · Daniel Kueh

Received: 4 November 2011 / Revised: 15 April 2012 / Accepted: 18 April 2012 / Published online: 11 May 2012

Abstract The central pattern generator for heartbeat in the medicinal leech, *Hirudo* generates rhythmic activity conveyed by heart excitor motor neurons in segments 3–18 to coordinate the bilateral tubular hearts and side vessels. We focus on behavior and the influence of previously undescribed peripheral nerve circuitry. Extracellular recordings from the valve junction (VJ) where afferent vessels join the heart tube were combined with optical recording of contractions. Action potential bursts at VJs occurred in advance of heart tube and afferent vessel contractions. Transections of nerves were performed to reduce the output of the central pattern generator reaching the heart tube. Muscle contractions persisted but with a less regular rhythm despite normal central pattern generator rhythmicity. With no connections between the central pattern generator and heart tube, a much slower rhythm became manifest. Heart excitor neuron recordings showed that peripheral activity might contribute to the disruption of centrally entrained contractions. In the model presented, peripheral activity would normally modify the activity actually reaching the muscle. We also propose that the fundamental efferent unit is not a single heart excitor neuron, but rather is a functionally defined unit of about three adjacent motor neurons and the peripheral assembly of coupled peripheral oscillators.

Keywords Central pattern generator · Peripheral innervation · Neuron · Oscillator · Leech

J. Jellies (✉) · D. Kueh
Department of Biological Sciences,
Western Michigan University,
Kalamazoo, MI 49008, USA
e-mail: john.jellies@wmich.edu

Abbreviations

AV	Afferent vessel
ANR	Anterior nerve root
CPG	Central pattern generator
FMRFamide	Phenylalanine-methionine-arginine-phenylalanine-NH_2
HE	Heart excitor
HT	Heart tube
IPSP	Inhibitory post-synaptic potential
Lav	Latero-abdominal vessel
Ldv	Latero-dorsal vessel
Llv	Latero-lateral vessel
M	Midbody segment
VJ	Valve junction

Introduction

A fundamental question in neurobiology is "How does a nervous system generate adaptive behavior?" One of the most intensively studied elements of the neural substrates of behavior has been a group of central neurons that produce rhythmic output to drive or entrain motor assemblies (Delcomyn 1980). Such central pattern generators have been reviewed extensively in the literature (Marder and Calabrese 1996; Stein et al. 1997). Central pattern generators are phylogenetically diverse including spinal rhythm generating networks for locomotion (Cohen and Wallen 1980; Grillner et al. 1998; Kiehn and Butt 2003; Rybak et al. 2006), networks involved in breathing, biting and chewing in vertebrates and invertebrates (Morgan et al. 2000; Lund 2011), swimmeret beating in crayfish (Hughes and Wiersma 1960; Ikeda and Wiersma 1964; Smarandache et al. 2009), the stomatogastic network in crustaceans

(Nusbaum and Beenhakker 2002; Saideman et al. 2007), swimming, courtship and heartbeat in leeches (Kristan and Calabrese 1976; Thompson and Stent 1976a, b, c; Stent et al. 1978; Weeks 1981; Calabrese and Maranto 1984; Maranto and Calabrese 1984a, b; Wagenaar et al. 2010; Chen et al. 2011).

A key attraction of central pattern generators as models for study has been the idea that their output can be studied as the product of the circuitry and synaptic interactions of a well-defined set of interneurons, and that they can generate complete activity patterns in isolation. Thus, an understanding of central pattern generators goes a long way toward addressing central questions pertaining to the neural bases of behavior. Nevertheless, central pattern generators alone are not sufficient to account for intact, complex behavioral patterns (Calabrese et al. 2011). There are many ways in which centrally generated activity can be modulated by sensory feedback (Heitler 1986; Deller and MacMillan 1989; Cang and Friesen 2000, 2002), sculpted by modulation (Dickinson et al. 1988; Morgan et al. 2000) and conveyed to effectors in ways that are filtered by electrical and mechanical properties of an assembly of efferents and muscles (Brezina et al. 2000). In addition, there has been recognition that the activity patterns generated by central pattern generators emerge despite substantial variability in underlying synaptic strengths and temporal patterning (Wenning et al. 2004b; Goaillard et al. 2009; Norris et al. 2011) compared to those seen in the actual behavioral output in intact animals.

In the present study, we have extended our understanding of the intensely studied rhythmic behavior that underlies coordinated contraction of bilateral heart tubes (HT) in the leech. This system is composed of a segmentally distributed network of heart interneurons that generate rhythmic oscillations used to phasically entrain segmentally iterated heart excitor (HE) motor neurons. The central pattern generator and HE neuron entrainment of heart contraction were first identified and described by Thompson and Stent (1976a, b, c) and the understanding of this circuit was substantially extended by Calabrese and Maranto (1984) and Maranto and Calabrese (1984a, b).

The leech has a closed circulatory system with two lateral tubular hearts that extend over the length of the animal (Hildebrandt 1988; Wenning et al. 2004a). The central pattern generator distributes a pattern of activity to HE neurons in segments 3–18 such that HE neurons fire bursts in either a rear-front pattern (peristaltic) or weakly front-rear pattern (synchronous) (Thompson and Stent 1976a; Maranto and Calabrese 1984b). These two modes switch sides every 20–50 beat cycles under the influence of central pattern generator elements (Thompson and Stent 1976a; Krahl and Zerbst-Boroffka 1983). The underlying mechanisms of switching, rhythm generation, premotor patterning, intersegmental coordination, and distribution of central activity have been intensively studied in this system (Norris et al. 2006, 2007a, b, 2009, 2011; Garcia et al. 2008).

In studies of blood flow, it has been determined that when one HT is in peristaltic mode, which generates relatively high-pressure constrictions, the other HT would be in a synchronous mode, which generates low-pressure constrictions (Hildebrandt 1988; Wenning et al. 2004a). Presumably, this difference leads to net driving forces that in conjunction with the closing of segmentally iterated HT sphincters perfuse various lateral capillary networks of the microvasculature. Also, the afferent vessels (AVs) have been found to contract to propel blood into the HT and that this, along with flow generated by the opposite HT as well as contractions of remote phase shifted segments of the ipsilateral HT, fills the HT during diastole (Wenning and Meyer 2007). However, several questions arise when attempting to link the very well studied centrally patterned activity and the coordinated pattern of segmental and intersegmental vessel contraction. For example, how do AV contractions consistently lead the HT if both are entrained by the same activity conveyed orthodromically by an HE neuron? How do variable burst patterns and intraburst frequencies in an HE neuron lead to consistent HT contractions? Finally, how are AV contractions linked to HT contractions?

To address these questions, we took advantage of the accessibility of both the peripheral and central circuitry in the heart system of the medicinal leech to characterize the coordinated contractions of AVs and HT. We present a model that accounts for previously observed, yet long unexplained antidromic neural activity (Thompson and Stent 1976a) and that generates predictions about how this peripheral network might be used to translate timing information from the central pattern generator into robust behavior. Rather than viewing a single segmental HE neuron as the output path, we propose that the minimum functional effector is an overlapping collection of about three adjacent HE neurons and the associated peripheral oscillators they conjointly entrain.

Materials and methods

Animals and preparations

Medicinal leeches, *Hirudo* spp. (Siddall et al. 2007) were obtained from a breeding colony established in the laboratory and operating for over 15 years. Breeding stocks were originally obtained and occasionally replenished from Leeches USA (Westbury, New York) and Niagara Leeches (Cheyenne, Wyoming). For these studies leeches were

6–18 months old, fed 3–5 times, and were 6–12 cm long, stretched-out.

Thirty-six leeches were used to generate these data across six procedures. In all cases, animals were anesthetized in ice-cold leech Ringer solution for dissection, then the cold solution was replaced with one at room temperature that was replaced thereafter about every 10–15 min. The Ringer solution was composed of (in mM) 115 NaCl, 4 KCl, 1.8 $CaCl_2$, 1.5 $MgCl_2$, 10 D-glucose, 4.6 Tris Maleate, and 5.4 Tris Base, pH 7.4 (Muller et al. 1981).

In the first procedure, 12 leeches were used to examine HT contractions under largely intact conditions to preserve innervation and hemodynamics. Leeches were stretched with ventral side up and pinned at anterior and posterior suckers. Then, 2–4 pins were used to secure one side through a layer of body wall pinched near the lateral midline so that pins would not puncture the body cavity while a small lateral stretch allowed us to make a shallow incision along the lateral midline on the opposite side. The incision cut through dermis and circular muscle, but did not penetrate the longitudinal muscle layer or the gut. The cut edge was reflected and pinned down. Fine forceps were used to separate the pigmented dermis and circular muscle layers from the body over 4–8 segments. When illuminated from above, this preparation allowed for clear visualization of HT and side vessel contractions. Since few capillaries were severed, blood loss appeared minimal and the system was operational with no obvious change in blood volume for several hours (though these experiments usually lasted 30 min). Baseline data were pooled from midbody segments 9–11 (M9–11).

The second procedure involved a dissected preparation to perform extracellular recording at the target. The animal was pinned dorsal side up and an incision made along the dorsal midline along the entire body through all layers. A group of nine leeches was used. The cut edges were pinned to the black wax substrate and gut contents were washed away with Ringer solution. The gut was peeled away from M8 to 12 and the anterior and posterior nerve roots in M1–8 and M12–21 were transected on the right side near the ganglion, leaving M9–11, as well as the contralateral side intact. All data were gathered from M10. Preliminary studies had revealed that innervation of three consecutive segments resulted in robust and coordinated contractions in the middle segment. Connective tissue was gently pulled away from the area between AVs and the HT in M10 using fine forceps. Data were gathered with M9–11 intact, then the nerve roots in M9 and M11 were transected and data were gathered again. Finally in this procedure, the nerve roots in M10 were transected and data gathered.

A group of three animals was used in a third procedure as a control for experimental rundown. Animals were dissected and prepared for valve junction (VJ) extracellular recording as described above except that all nerves remained intact. An electrode was placed on the VJ at M10 and optical recordings of latero-dorsal vessel (Ldv) and HT were obtained. For this procedure, the data were gathered for about 30 min without changing Ringer or making any adjustments to the electrode or fiber optics. To assess possible influences of rundown, we expressed measures from the last 3 min (e.g., HT frequency) as a function of the same measure from the first 3 min. A ratio of 1 indicates no change.

In a fourth procedure, the leeches were prepared as above, but to obtain intracellular recordings from the HE, each animal ($n = 6$) was re-pinned ventral side up and small windows cut through the body wall above M9–11 to expose the central nervous system. The edges of the tissue windows were stabilized with small pins and a second shallow incision was made at the lateral midline to peel back the pigmented skin above the HT in M10 to visualize the HT. This preparation was pinned in a Sylgard-coated dish so that each ganglion could be viewed with dark-field illumination from below to guide intracellular impalement while the HT was illuminated from above for optical recording of contraction. Data were gathered as above with sequential nerve cuts.

In the fifth procedure, four leeches were prepared for extracellular recording as described above. In this procedure, HT contractions at M10 were recorded from homologous locations on both sides simultaneously.

A sixth procedure was developed to directly confirm that VJ regions were initiation sites of antidromic action potentials. We prepared two animals for extracellular recording. In these preparations, nerve roots on the right side were transected in M1–8, M10 and M12–21 and suction electrodes were placed on the VJ at M10 and on the cut anterior nerve root at M10 close to the central nervous system. Once bursts of action potentials and optical recordings of HT were reliably obtained, nerve roots in M9 and M11 were transected and data were again gathered.

Recording muscle contractions

All experiments were carried out using a trinocular dissecting microscope fitted with a color CCD video camera with video images captured using IC Capture 2.1 (The Imaging Source, Charlotte, NC, USA). Images of the experimental field were viewed on a 12 in. flat panel color monitor at magnification sufficient to clearly distinguish contractions of both HT and AVs. To record HT and AV contractions, we fabricated analog optical detectors after those used by Pickard and Mill (1974). The detector consisted of a standard infrared phototransistor (RadioShack) in series with a 10 kΩ resistor and a 9 V battery. The voltage across the resistor thus depended upon illumination

of the phototransistor, which was digitized by a PowerLab 26T and recorded with LabChart 7 (ADIinstruments, Colorado Springs, CO, USA). These data are referred to as optical signals.

To selectively monitor behavior at particular locations at the HT and AV, it was necessary to mask irrelevant areas of the monitor image. To accomplish this, we coupled the phototransistor to the image using a 2–3 mm diameter jacketed acrylic fiber optic about 15 cm long. The open end of the fiber was positioned in front of the monitor and the position was adjusted to obtain the maximal signal. Usually, this was about 1–2 mm from the face of the monitor. In all records, an upward deflection indicates a contraction.

Electrophysiological recording

Intracellular recordings from individual neurons were obtained using glass microelectrodes (resistances of 45–75 MΩ, filled with 1 M potassium acetate) and standard electrophysiological techniques (World Precision Instruments 773 preamplifier). Signals were simultaneously viewed on a Tektronix oscilloscope and digitized by a PowerLab 26T (ADInstruments, Colorado Springs, Colorado) at 10,000/s. Direct current (0.1–0.4 nA hyperpolarizing) was injected through the bridge circuit of the amplifier to silence the neuron in the central nervous system for a period of 30–90 s. To cut the nerve roots, it was necessary to withdraw the electrode and re-impale the same neuron. Therefore, a 5-min recovery time was allowed before data were captured. Only impalements that showed consistent stable resting potentials (30–45 mV) were used.

Extracellular recordings were obtained by placing a suction electrode on the junctional area joining an AV to a HT. While similar recordings could be obtained from both afferent lateral vessels, latero-dorsal (Ldv) and latero-lateral (Llv), we limited these studies to the Ldv–HT junction, here referred to simply as the VJ. Electrodes were fabricated from 1 mm diameter electrode glass (WPI, Sarasota, FL, USA) pulled to a taper and broken by hand. The tip was fire-polished to a diameter of 30–40 μm, checked by comparing the opening to tungsten wires about 25 and 50 μm in diameter. The external reference wire was Teflon-coated fine silver with the exposed tip coated with silver chloride.

Extracellular signals were obtained using SpikerBox differential amplifiers that were built from kits (Backyard Brains, Ann Arbor, Michigan) (Marzullo and Gage 2012). These amplifiers were unfiltered and all differential recordings were obtained without grounding the bath. The only modifications made to these amplifiers included disconnecting the speaker and fabricating input and output cables. The utility of these amplifiers was checked first by obtaining extracellular recordings of action potentials en passant from well-studied dorsal-posterior nerves (not shown). These nerve signals were used to confirm that adequate signals could be obtained in this fashion and digitized (4,000/s) using the PowerLab 26T.

Data analysis

Continuous records were obtained for 2–10 min. For analysis, continuous segments of 2–5 min were chosen. The most consistent optical signal recorded was the upward deflection that corresponded to the initiation of contraction. Thus, each sharp upward inflection was used as a marker for timing of contraction. While the records may also be a valid reflection of duration and relative magnitude of contraction, these optical recordings were not calibrated for those parameters.

Analysis was carried out manually using the marker tool in LabChart 7. When the marker was placed and the cursor moved to position, the time interval recorded to the nearest 0.1 s. Since the behavior was cyclical, each sequence of measures could include up to 80 replicate measures. For most analyses, replicates were averaged. n was the number of animals from which those replicates derived (12, 9, 3, 6 or 4 as described above). All data are reported as mean ± SEM.

To determine the relative phasing of the Ldv and HT relative to the VJ, a phase plot was constructed based in part on the methods of Thirumalai and Marder (2002) and Norris et al. (2006). Unlike the duty cycle of a VJ, which was identified as a burst of multiple action potentials, the duty cycle of an Ldv and HT was identified as the duration of a contraction (a positive amplitude in the optical trace). The beginning of a contraction was defined as the on-phase, whereas the end of a contraction was defined as the off-phase. If the VJ bursts produced a series of corresponding contractions in the Ldv or HT, these series of contractions would be counted as one duty cycle. Intervening contractions that do not correspond to a VJ duty cycle and appeared myogenic were ignored. The positions of on- and off-phases from an Ldv or HT duty cycle were normalized to the first action potential of a VJ duty cycle (set as marker driver), using the phase (ϕ) equation:

$$\phi = \left(\frac{t_x - t_{\mathrm{VJ}}}{T_{\mathrm{VJ}}} \times 100 \right)$$

In the ϕ equation, t_x is the time (in ms) of the on- or off-phase of a VJ, HT, or Ldv duty cycle whereas t_{VJ} is the time (in ms) of the first action potential of a corresponding VJ duty cycle. T_{VJ} is the cycle period of the VJ, which was defined as the duration between the first action potential of a VJ duty cycle and the first action potential of a subsequent VJ duty cycle. The position of the first action potential in the VJ duty cycle was set at 0 %.

In addition to the phase plot, all other average-dependent measures for each condition were expressed in terms of frequency (in cycles/min), latency (in s), burst durations (in s), and intercycle period [in s or in standard deviation divided by the mean (SD/mean)]. Given that each animal was exposed to all treatment conditions within a procedure, within-subject analyses were used to determine significant differences. If there were only two conditions for each a measure, a paired *t* test was used. If there were three or more conditions for each measure, then a repeated-measures ANOVA was used. Data from experiments that involved surgical manipulations as well as multiple simultaneous recordings were analyzed using a two-factor repeated-measures ANOVA, with the number of intact nerves and type of recording as the two factors. If necessary, the data were also analyzed with a non-parametric equivalent. When significant differences were found, a post hoc analysis with Tukey was conducted. Significant differences were defined as $p < 0.05$ for all tests. Graphs were constructed with Adobe Photoshop CS3 (Adobe Systems Inc., San Jose, CA, USA) while statistical analyses were performed with SigmaPlot 10 (Systat Software, Inc., Point Richmond, CA, USA).

Results

Segmental behavior of the HT

Rhythmic contraction of the HT generates the pressure gradients needed to circulate blood throughout microvasculature (Fig. 1). The leech has 32 body segments, the middle 21 of which are termed midbody (Muller et al. 1981). The HT is a bilaterally paired muscular tube that extends through the entire midbody near the lateral midline and consists of segmentally iterated modules (Hildebrandt 1988) of two AVs and one efferent vessel (Fig. 1a). Each of the AVs (Ldv and Llv) is associated with a specialized junctional region where it joins the HT and has dense, non-contractile finger-like internal projections that function as valves (Hildebrandt 1988). The efferent side vessel (latero-abdominal, Lav) is different in that it is narrower, directed toward the ventral midline and contains a sphincter-like region that restricts blood flow in both directions when closed (Hildebrandt 1988). Blood flow has been analyzed in some detail (Hildebrandt 1988; Wenning et al. 2004a; Wenning and Meyer 2007). Generally, blood enters the segmental HT from capillaries via the Ldv and Llv and

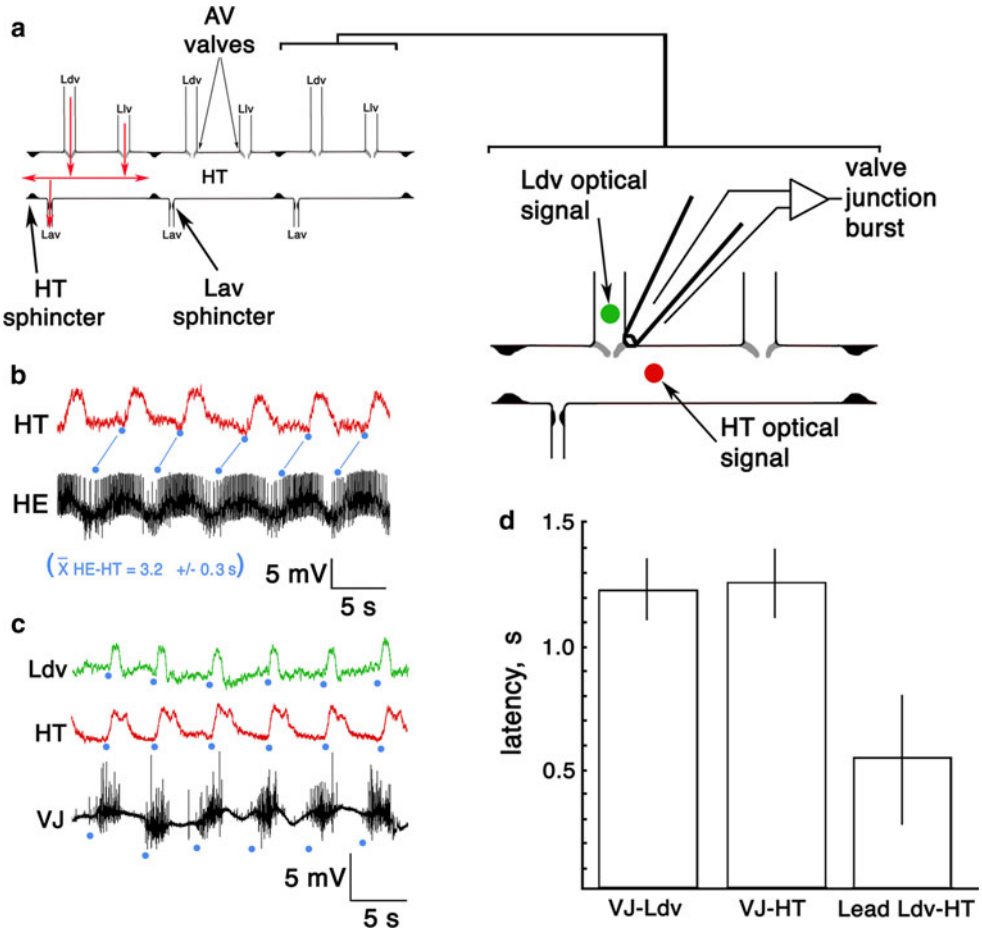

Fig. 1 Coordinated and entrained contraction of afferent side vessels (*AVs*) and heart tube (*HT*). **a** Diagram of three adjacent segments of HT illustrating segmental iteration of modules. *Red arrows* indicate normal blood flow, which can be in either direction in the HT. To the right is shown an expansion of one segmental module as an illustration of electrode and fiber optic placement for gathering data. **b** Individual bursts of action potentials (*black*) from an HE neuron is followed by a corresponding contraction (*red*) in the ipsilateral HT. Each *blue line* represents a latency from the first action potential after the depolarizing voltage inflection (*blue dot*) to the rapid upward inflection in the HT trace related to contraction initiation (*blue dot*). **c** Representative record of simultaneous recording of Ldv (*green*) contraction, HT (*red*) contraction and the VJ burst of extracellularly recorded action potentials (*black*). **d** Temporal latencies between the events. VJ bursts led both Ldv and HT while Ldv led HT

exits via the Lav (red arrows Fig. 1a), and blood also moves anterior–posterior through the HT. In peristaltic mode, blood moves posterior to anterior for 20–50 cycles and then switches to a more synchronous mode that conveys blood in the opposite direction (Thompson and Stent 1976a) (the double-headed arrow Fig. 1a).

Contraction of the HT is entrained by rhythmic activity of a segmentally iterated HE neuron (Fig. 1b). The rate of this activity was found to be between 8 and 15 cycles/min, which was imposed upon the HE neuron by the central pattern generator based on the rhythmic barrage of hyperpolarizing inhibitory postsynaptic potentials (IPSPs) that reflect the activity of the central pattern generator. Less well studied and not understood are the coordinated contractions of the innervated AVs. We found that contractions of the midbody Ldv were substantially coordinated in advance of the HT (Fig. 1c, d). When we separated contractions that led HT from all other contractions, we found that the average Ldv frequency was higher than the average HT frequency (Fig. 1d). However, we found no significant difference in frequency between leading Ldv and HT and, under orthodromic central pattern generator entrainment, about 75 % of all Ldv contractions led the HT by an average of 0.5 ± 0.3 s in the dissected procedure (Fig. 1d). This was not different from the latency seen in the procedure with minimal dissection (0.7 ± 0.1 s). Time lagging Ldv contractions accounted for about 25 % of all contractions and most often occurred during the active contraction of the HT in a rapid sequence of double contractions (not shown). Although we did not routinely separate the behaviors into peristaltic or synchronous modes, we were able to observe these behaviors in both modes. Any subtle quantitative differences might be examined in future studies.

To determine if activity patterns change over time due to rundown, we recorded from three animals with all nerves intact, using room temperature Ringer's solution and not changing it for the duration of the experiment. Contractions in these animals slowed slightly, but remained coordinated for 30 min, which was confirmed by dividing measurements made in the final 3 min by comparable measurements made in the first 3 min. In this way, a ratio of 1 would indicate no change. HT frequency was 0.86 ± 0.06 cycles/min, Ldv frequency was 0.86 ± 0.16 cycles/min and VJ burst frequency was 0.87 ± 0.01 cycles/min. Thus, while there was a modest slowdown, it was the same across each of these three measures. We also examined VJ burst duration, which showed no change (1.08 ± 0.07 s). Thus, the specific effects seen in the results cannot be the result of rundown over time.

Electrical activity at the valve junction

Innervation of the HT has been described, as has synaptic entrainment of the circular muscle leading to contraction (Thompson and Stent 1976a; Maranto and Calabrese 1984a; Calabrese and Maranto 1986). One of our interests was to examine how the side vessel contractions were coordinated to form the more complete behavior. In previous work, we showed that HE neurons not only innervated the entire HT and AV via small varicosities, but they also provided discrete, dense focal innervation of both the Ldv and Llv junctions (Kueh and Jellies 2012). To address the potential role of the presynaptic terminals at these junctions and how they may couple the activity in the AVs to the contractions of the HT itself, we obtained optical recordings of the Ldv and HT (within 1 vessel diameter of the junction, Fig. 1a) and simultaneously recorded extracellularly from the innervated VJ. All optical and electrical records were obtained from midbody segment 10 (M10). At the beginning of these experiments, nerve roots at M9 and M11 were left intact. We recorded large discrete bursts of action potentials (or very large, rapid passive potentials) at the VJs that occurred in advance of the contractions of these vessels (Fig. 1c, d). We were unable to record comparable bursts from either the HT or at the Lav junction with HT using the techniques described here. While the VJ bursts were large, discrete, and composed of many individual units, we did not examine the structure of the bursts in the work presented here. This will be examined in future work. For measuring latency, we selected the first action potential of the burst (an initial action potential was defined as a rapid voltage change within 50 ms of the next action potential).

Sequential changes in coordination and frequency

When nerve roots from three adjacent midbody segments were left intact, the pattern of VJ bursts closely resembled the activity patterns of entrained HE neurons in rhythmicity, cycle, and temporal relationship to vessel contractions. It is not known if these VJ bursts represented action potentials recorded pre-synaptically from HE neurons, action potentials in VJ cells, large rapid post-synaptic potentials, or a combination of all three. Nonetheless, a relationship between the VJ burst and HE neuron activity could be inferred based on the onset and duration of both activity patterns. The innervation territory of HE neurons established during early development is such that each HE neuron extends at least 1 segment anterior and 1 segment posterior in addition to innervating the segment of origin (Jellies et al. 1992). This pattern persists in postembryonic leeches (Kueh and Jellies 2012). We also found in preliminary experiments that reducing the territory receiving innervation by HE neurons to less than three adjacent segments seemed to compromise the HT frequency. We employed the extracellular procedure to examine sequential reduction in innervation from the central nervous system (Fig. 2).

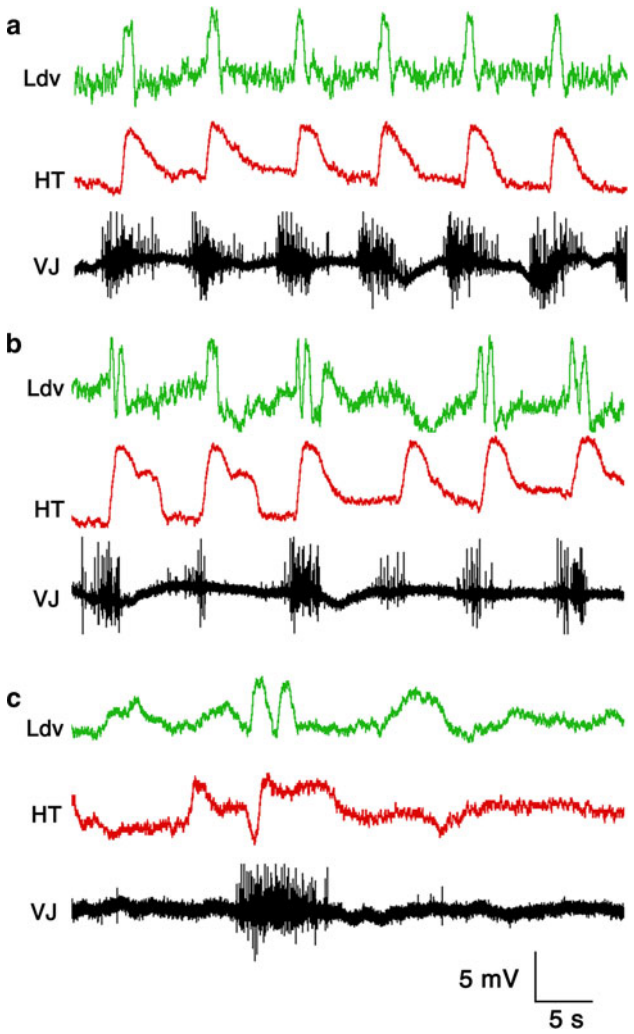

Fig. 2 Simultaneous recordings of contractions from the Ldv and HT as well as bursting activity from the VJ at M10. **a** When nerve roots from M9, M10 and M11 were intact, each Ldv and HT contraction consistently coincided and followed each VJ burst. **b** When nerve roots from M9 and M11 were cut, the number of Ldv contractions that failed or lagged became apparent. **c** When the one remaining set of nerve roots from M10 was cut, LdV and HT contractions would either occur without VJ activity or would follow VJ bursts. Each VJ burst coincided with a doublet Ldv and single HT contraction

When nerve roots from M9 to 11 were intact, the VJ, Ldv, and HT activities appeared to be coordinated (Fig. 2a). Without moving the suction electrode, nerve roots in M9 and M11 were cut and data were again collected 1–5 min later (Fig. 2b). With just one HE neuron projecting to the HT, there remained substantial entrainment of the HT at that segment, but at a noticeably reduced frequency. There was also a change in Ldv contractions, which showed some total failures (Fig. 2b) as well as more Ldv contractions that seemed to lag HT.

We then transected the remaining nerve roots in M10, leaving the entire right side of the animal denervated. As expected, the frequency of HT contractions and VJ bursts on the right side of the animal dropped precipitously (Fig. 2c). When VJ bursts occurred, they still led contractions of both Ldv and HT (Fig. 2c). Nevertheless, both Ldv and HT could exhibit spontaneous contractions in the absence of a VJ burst (Fig. 2c).

We quantified these changes across each of the three conditions in the procedure (Fig. 3) finding that with just one HE neuron entraining the HT (M10 intact), HT frequency decreased significantly ($p < 0.05$, Tukey). Leading Ldv contractions decreased significantly compared to control (9, 10, 11) and total Ldv (all $p < 0.05$, Tukey). Somewhat unexpectedly, there was also a significant increase in VJ burst duration (Fig. 4; $p < 0.001$) when all central entrainment was removed.

Eliminating adjacent orthodromic entraining signals also compromised coordination between AV and HT and this corresponded to a reduction in VJ frequency. To illustrate this, we constructed a phase plot using the VJ burst as a reference (Fig. 5a). Compared to control in which nerve roots from M9 to 11 (9, 10, 11) were intact, we found no significant differences in the mean on-phases of Ldv and HT at each progressive nerve transection, suggesting that when a VJ burst occurred, it retained its consistent phase advance with the Ldv and HT. Nevertheless, mean duty cycle and off-phase of all three activities decreased significantly with each progressive nerve transection, which we attributed to the increased cycle periods. Moreover, the increased cycle periods of Ldv and HT in the phase plot when all nerves were transected were due in part to the

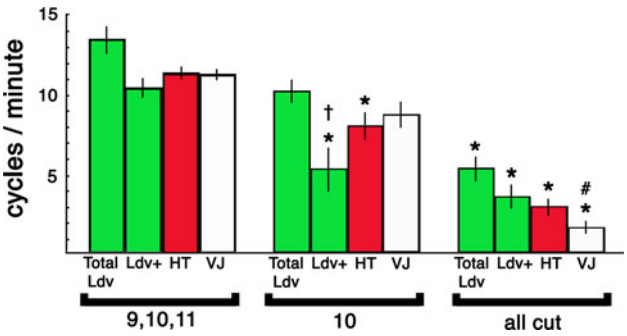

Fig. 3 Changes in the frequency of Ldv and HT contractions and VJ burst with sequential reduction in orthodromic entrainment. No significant differences in average frequency were observed between the four different recordings when nerve roots at 9, 10, 11 were intact. When only the nerve roots from M10 were intact, the average frequency of leading Ldv (Ldv+) and HT contractions decreased significantly relative to the average frequency of Ldv+ and HT contractions when nerve roots at 9, 10, 11 were intact. Finally, when all nerve roots were cut, the average frequencies from all four recordings decreased significantly compared to the average frequencies from all four recordings when nerve roots at 9, 10, 11 were intact. *Error bars* represent ±SEM. Significant difference from total Ldv within condition, $^{\dagger}p < 0.001$. Significant difference from VJ in 10 intact, $^{\#}p = 0.004$, Tukey. Significant differences from 9, 10, 11 intact, $^{*}p < 0.05$, Tukey

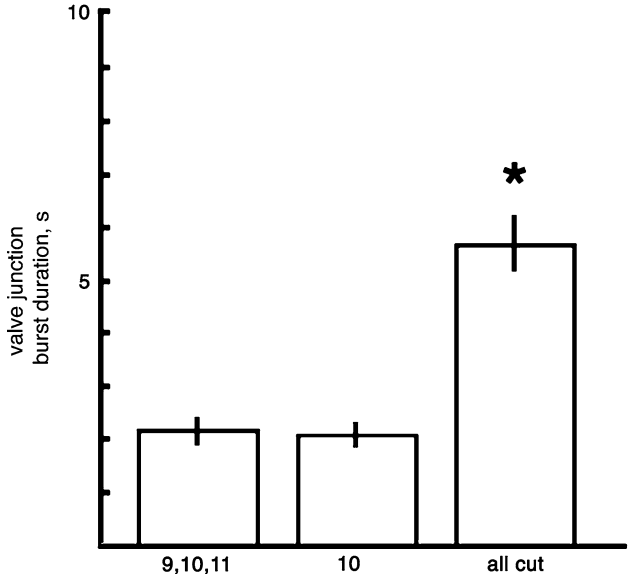

Fig. 4 Change in burst duration. The duration of the VJ burst remained constant with any orthodromic entrainment (9, 10, 11 intact and 10 intact), but on average increased twofold to threefold in the absence of entrainment (all cut), $*p < 0.001$

intervening series of Ldv and HT contractions between each VJ burst (e.g., Fig. 5b) being excluded from the phase plot. Since these spontaneous contractions of Ldv and HT were not related to VJ action potentials or in any simple way to each other, we suggest that they are independently myogenic. To further characterize this outcome, we compared their latencies (Fig. 6). The first cluster data are repeated from Fig. 1. Ldv contractions with reduced innervation often occurred throughout the cycle, leading to a large increase in average latency with a pronounced increase in variability.

An important feature of the HT beat cycle not addressed by averages of frequency is regularity. There are two possible predictions. One prediction is that the frequency may decrease, but do so regularly with evenly spaced period between each cycle. Alternatively, the average frequency may decrease by having multiple cycles with regular periodicity interrupted by sequences of cycles with significantly different periods. To distinguish between these two predictions, we measured each HT period, cycle by cycle across all replicates in all nine animals. When all nerves were cut, the average ± SEM intercycle period of 23.2 ± 6.6 s increased significantly relative to the average intercycle period of 5.5 ± 0.2 s when all three nerves (9, 10, 11) were intact ($p < 0.05$, Tukey) (Fig. 7a). Similar trends were observed when the intercycle period was expressed in terms of SD/mean ($p < 0.05$, Tukey) (Fig. 7b). These results support the second prediction and indicate that with loss of innervation and central pattern generator entrainment, there was a change from a regular rhythm to one that was more irregular and that showed loss of contraction cycles when some innervation was intact as well as myogenic contractions when all nerves were transected.

Orthodromic and antidromic activity

Since it appeared that there was a peripheral oscillator at the VJ, and that decreasing the degree of segmental orthodromic entrainment resulted in both a decrease in HT and Ldv frequency as well as uncoupling of Ldv and HT,

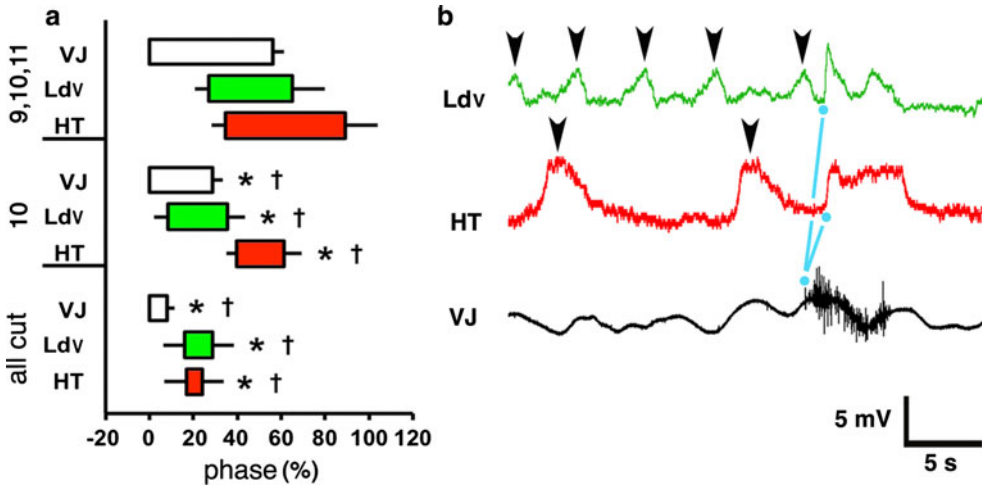

Fig. 5 VJ bursts couple Ldv and HT contractions. **a** Phase relationships between VJ, Ldv, and HT. The beginning of a rectangle represents the mean on-phase whereas the end of a rectangle represents the mean off-phase. The length of each rectangle represents a duty cycle. The scale of 0–100 % corresponds to the duration of a VJ cycle period. *Error bars* represent ±SEM. Compared to preparations with all three nerves (9, 10, 11) intact. *Asterisk* represents a significant difference in duty cycle whereas *dagger symbol* represents significant difference in off-phase ($p < 0.05$). **b** Select record of Ldv, HT and VJ with all nerves transected showing numerous spontaneously occurring contractions (*arrowheads*) not associated with VJ burst. *Blue dots* and *lines* show the relationship of a spontaneous VJ burst and the associated phase relationships with Ldv and HT contractions

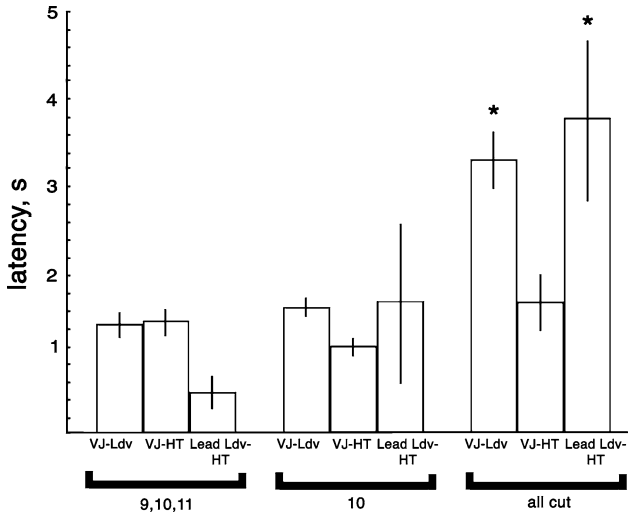

Fig. 6 Uncoupling of coordinated contractions with reduction of orthodromic entrainment. Latency relationships between VJ burst and leading Ldv (Ldv+), VJ burst and HT, and Leading Ldv and HT are illustrated in the first cluster with three segments of orthodromic entrainment, 9, 10, 11 intact. With a single segment (M10) intact, there was a significant reduction in VJ–HT coupling and Ldv–HT coupling. Following cutting all the peripheral innervation there was little evidence of coordination among the VJ bursts, Ldv and HT in any combination (*last bracket*). *Asterisk* represents a significant difference from 9, 10, 11 intact, $p < 0.001$

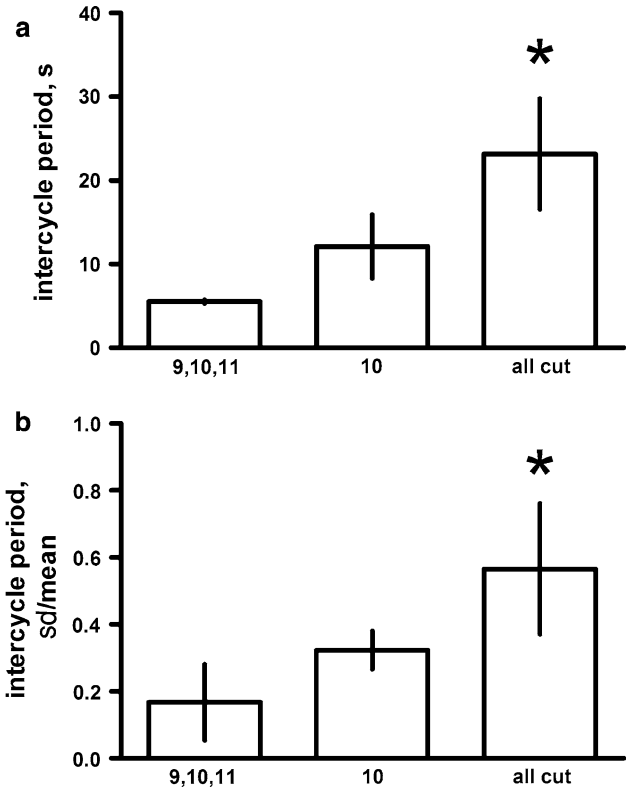

Fig. 7 Regularity of rhythmic activity decreased with reduction of orthodromic entrainment. **a** The average intercycle period (s) when all nerves were cut was significantly greater than the average intercycle period with three segments of nerves (9, 10, 11) intact. **b** Similar trends were observed when the average intercycle period was expressed in terms of SD/mean. *Error bars* represent ± SEM. Significant difference from three segments of nerves intact (9, 10, 11) intact, $^*p < 0.05$

we designed experiments to replicate the nerve cuts, but using intracellular recording from the HE soma instead. As would be expected if the entrained VJ activity was directly related to HE neuron activity, we observed a pattern of changes in the HE–HT relationship with sequential reduction of orthodromic entrainment directly comparable to that seen in the VJ–HT procedure (compare Fig. 8a–c with Fig. 2a–c).

With only one axon from single HE neuron intact (Fig. 8b), there appeared to be a reduction in HT contraction frequency, yet there were no significant changes in the frequency of central pattern generator entrained HE bursts (Fig. 9a). To replicate the condition whereby all nerves were cut, we injected hyperpolarizing current through the balanced bridge into the soma of the remaining HE at M10 (Fig. 8c). This resulted in periodic, long (Figs. 8c, 9c) bursts of antidromic action potentials that closely resembled the burst seen at VJ when all orthodromic entrainment was removed (see Fig. 2c). Interestingly, the average latency between the initial antidromic action potential in this extended burst and HT contraction was significantly shorter than that seen with orthodromic entrainment (Fig. 9b; $p < 0.001$).

In a novel experiment, we silenced the HE neuron centrally in M10 while the innervation from adjacent M9 and M11 was intact (Fig. 8d). After 2–3 cycles of no HE neuron activity (but continued HT contraction), rhythmic bursting of antidromic action potentials in HE(M10) was seen. There was no significant difference between the frequency of antidromic bursts and the HE neuron bursts seen in intact conditions (Fig. 9a). Likewise, burst duration in the HE neuron was comparable to that seen for VJ bursts when the HT contractions were entrained orthodromically by central pattern generator activity (compare Fig. 9b, c with Figs. 3, 4) while latency was intermediate (Fig. 9b; $p < 0.05$). Finally, in these hyperpolarizing experiments, 5 of the 6 preparations showed clear bursts of rhythmic IPSPs that we inferred was a reporting of central pattern generator activity, which appeared to be cycling at the normal, predicted rate (Fig. 9a).

To confirm that action potentials initiated in VJ were conducted antidromically, extracellular records were obtained in two additional preparations with nerve roots in M1–8, M10 and M12–21 transected (Fig. 9d). As expected, bursts were recorded at VJ and these occurred before HT contraction. They also occurred before the burst, recorded some distance away toward the central nervous system. The nerve roots in M9 and M11 were then transected, giving rise to the expected long duration burst in VJ that

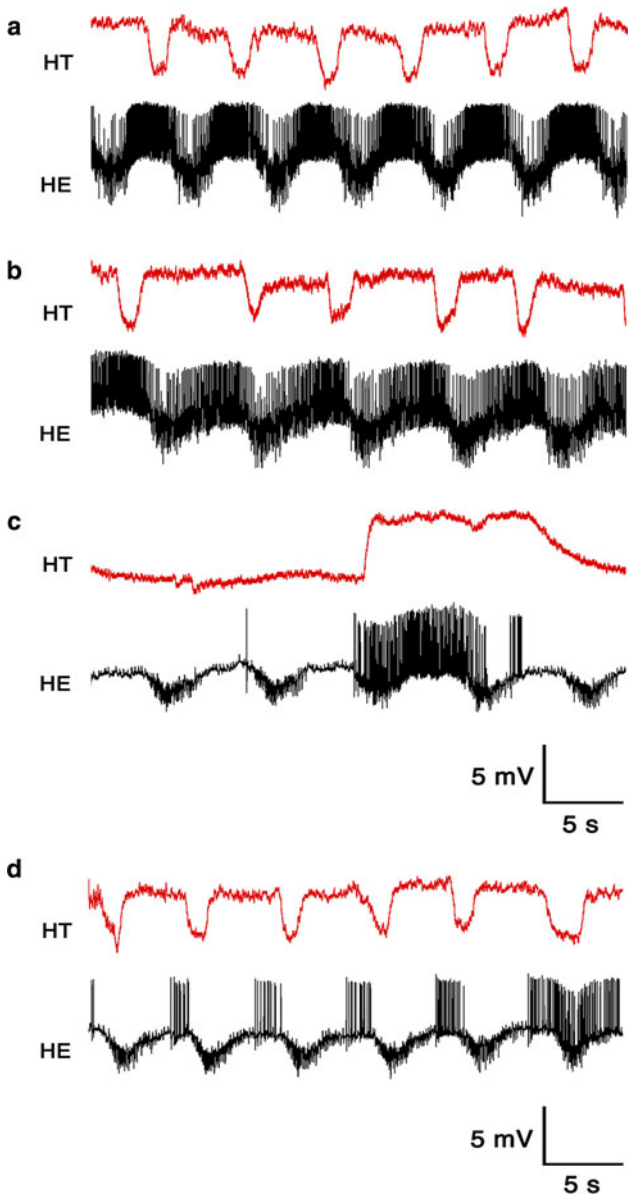

Fig. 8 Effects of sequential nerve cuts and intracellular hyperpolarization in reducing orthodromic entrainment. **a** With nerve roots from M9, M10 and M11 intact, the expected relationship between HE activity and HT contractions was observed. **b** Transecting the nerve roots in M9 and M11 resulted in a small decrease in frequency of both HE bursts and HT contractions with a reduction in regularity as expected from the previous experiments (Figs. 2, 7). **c** With only nerve roots from M10 intact, the HE was hyperpolarized to prevent orthodromic action potentials. A single orthodromic action potential (distinguished by having an after-hyperpolarization rather than rising directly from the baseline) occurred about 7 s before the spontaneous, long duration antidromic burst. This condition was experimentally equivalent to all nerves cut in the preceding experiments (Fig. 2). **d** Before cutting the nerves from M9 and M11, HE(M10) neuron was silenced by hyperpolarization. There were occasional longer bursts but the activity was dominated by the shorter bursts

again preceded both the HT contraction and the burst recorded from the anterior nerve root near the central nervous system (Fig. 9e).

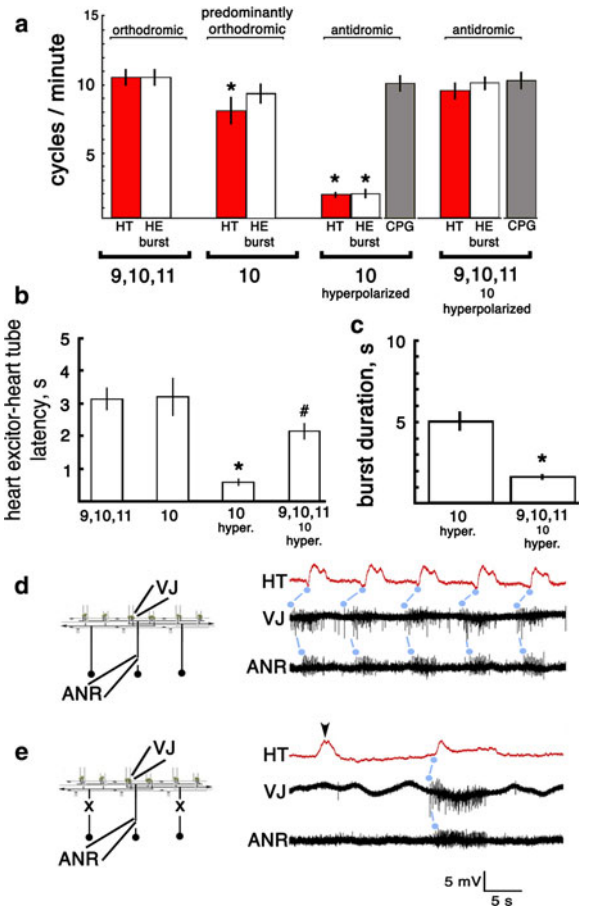

Fig. 9 Activity relationships during sequential elimination of orthodromic entrainment by cutting and hyperpolarization. **a** A notation is made above each cluster as to whether casual inspection showed the action potentials in HE to be orthodromic, or antidromic. When the single pathway of entrainment was removed by hyperpolarization (third cluster, 10 hyperpolarized), there was a significant decline in the average HT and HE frequencies. The *gray bar* represents the central pattern generator frequency inferred from the rhythmic bursts of IPSPs seen during hyperpolarization (see traces in Fig. 8). In the fourth cluster (9.10, 11, 10 hyperpolarized), the middle of three otherwise intact pathways was hyperpolarized and frequencies of HE bursts and HT contraction were observed not to be significant from the CPG frequency. *Error bars* represent ±SEM. Significant difference from 9, 10, 11 intact, $*p < 0.05$. **b** When the single HE that remained connected was hyperpolarized (10 hyperpolarized), there was a significant reduction in the average latency from HE burst to HT contraction. In the novel experiment having three adjacent intact pathways but hyperpolarizing the middle one (9, 10, 11, 10 hyperpolarized), the latency was observed to be significantly reduced compared to the condition with just one HE connected (10 hyperpolarized). Significant difference from 9, 10, 11 intact, $*p < 0.001$. Significant difference from 10 intact, $^{\#}p < 0.001$. **c** Comparing burst durations between the two conditions where HE10 was hyperpolarized revealed that the burst in HE10 was 2–3 times longer, $*p < 0.002$. **d** VJ bursts preceded both the HT contraction and the antidromic burst recorded from the anterior nerve root near the central nervous system. *Blue dots* and *lines* denote relationships of initiation of each event. **e** Spontaneous, long VJ burst occurred before the HT contraction and the antidromic burst recorded in the anterior nerve root near the central nervous system. *Blue dots* and *lines* denote relationships of initiation of each event

Bilateral independence

If the central pattern generator continues to oscillate at a relatively fixed frequency, even when the frequency of entrained HT contractions was reduced, then the frequency of HT contractions on the unoperated side should be unaffected by nerve transections. To test this, we repeated the nerve cut procedure while monitoring contractions of HT bilaterally (Fig. 10). When the nerves from M9 to 11 were intact, we saw the expected central pattern generator entrainment of left and right HTs (Fig. 10a, d). As expected, cutting nerve roots from all but the HE(M10) on the right side (leaving all nerves on the left intact) resulted in a decrease in HT and VJ frequency on the right (Fig. 10b, d), but in no significant change in HT frequency on the left. Finally, when all orthodromic entrainment was eliminated from the right side, the frequency of both VJ and HT dropped significantly ($p < 0.05$, Tukey) on the right side while the HT frequency on the left remained essentially unchanged (Fig. 10c, d).

Discussion

The behavior that is functionally appropriate for the leech circulatory system involves both the intersegmental HT contractions and the coordinated contractions of side vessels (Hildebrandt 1988). Most studies have concentrated on the regulation and phasing of HT contraction alone and on the mode switching that is controlled within the central nervous system. In the present study, we characterize one of the three side vessels as well as the peripheral innervation. Our results show that focal peripheral oscillators at specialized VJs between afferent side vessels and HT may be coupled by intersegmental axons from HE neurons and that the VJs can generate antidromic action potentials. We suggest that these strategically located peripheral oscillators are able to link contractions of AVs to the HT and insure that AV contracts consistently just before HT, supporting blood flow. We also predict that the activity actually reaching muscle to entrain contractions might be different than that expected from individual bursts of action potentials recorded from HE neurons centrally and we propose future studies to explore how to test this prediction.

While studies of centrally generated activity patterns have been enlightening, explaining functional behavior in terms of centrally generated patterns alone is often a challenge (Wenning et al. 2004b). While the central pattern generator in the leech is well understood, there are still variable aspects of synaptic activation that give rise to individual animal solutions to premotor patterning (Calabrese et al. 2011) and the fictive behavior often does not precisely match constriction patterns. Possible peripheral

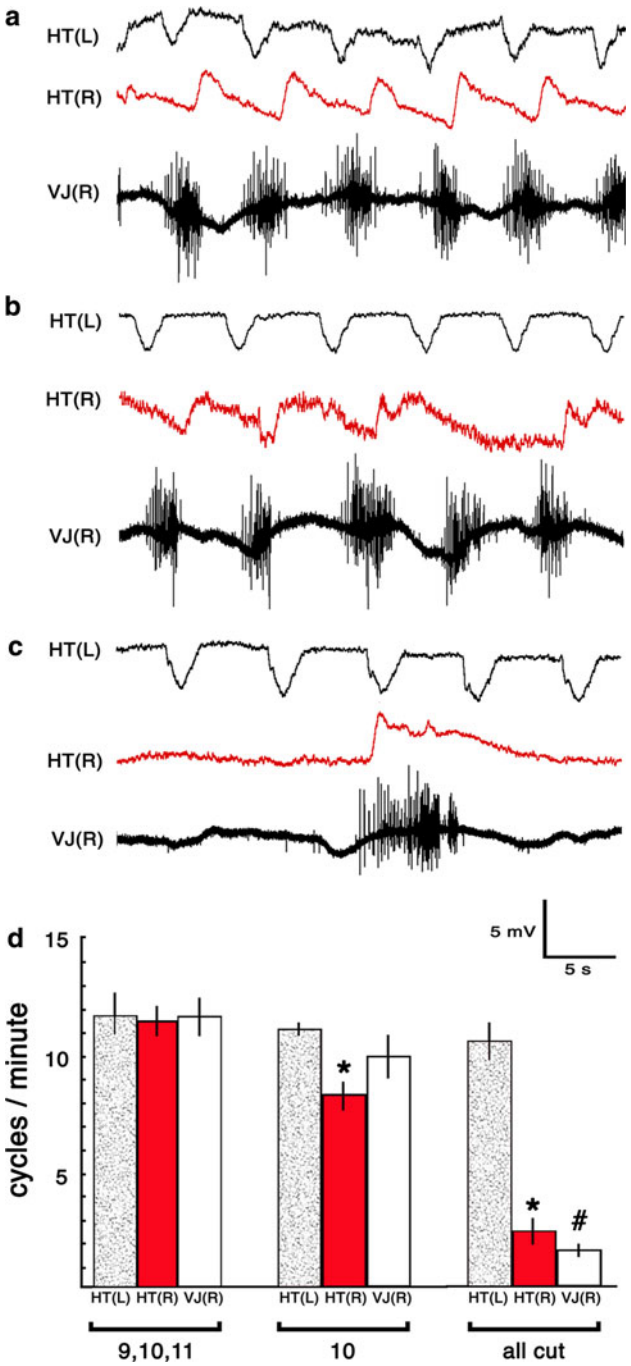

Fig. 10 Independence of HT contractions across the midline. **a** Nerve roots in M9, M10 and M11 intact on right side. Recording extracellularly from VJ and optically from HT similarly to the arrangement shown in Fig. 1, but instead of recording Ldv we recorded from a homologous HT location in M10 on the contralateral (left *L*) side. **b** Recording HT and VJ activity after nerve roots M9 and M11 were transected. **c** Recording HT and VJ activity with all nerves transected on the right side, all nerves intact on the left. **d** Changes in frequency with nerve transection; $^{*}p = 0.003$, $^{\#}p < 0.001$

influences such as muscle mechanics and hemodynamics have been suggested to account for this lack of matching (Wenning et al. 2004b). While there is also evidence in the

leech that activation of the Leydig cell can alter central pattern generator rate (Arbas and Calabrese 1990), there is no direct evidence that sensory feedback from HT contractions modulates the phase or frequency of the central pattern generator. Our data support this lack of feedback to the central pattern generator. First, as orthodromic entrainment was reduced by transecting nerves, the periodicity became progressively less regular (Figs. 5, 7) but did so by maintaining stretches of regular rhythmicity interrupted by loss of cycles. This implies that the central pattern generator maintained its regular rhythm in the background. The rhythm, therefore, does not normally require peripheral feedback to maintain a rhythm. In addition, as the HT contractions slow when nerves are transected, the central pattern generator does not change in frequency (Figs. 9, 10).

Peripheral network

We present elements of a model in Fig. 11 based on the results presented here. This model is very similar to the most complex and, therefore, seemingly less likely interpretation originally put forward by Thompson and Stent (1976a). Two key anatomical features of the model are shown in Fig. 11a, b. It has long been known that HE neurons contain and release acetylcholine to evoke an ionotropic response in HT muscle cells (Calabrese and Maranto 1986). HE neurons also use the peptide FMRFamide (Phenylalanine-Methionine-Arginine-Phenylalanine-NH_2) as a co-transmitter (Kuhlman et al. 1985a, b; Li and Calabrese 1987). We recently discovered a previously undescribed focal innervation of the VJ regions by peptide-negative presynaptic terminals belonging to HE neurons (Fig. 11a) (Kueh and Jellies 2012). It was this discovery that led us to record from the VJ regions. We suggest that these heavy clusters of peptide-negative terminals converging at VJs generate a rapid phasic response in VJ cells, and are part of the source of both the VJ bursts and the antidromic action potentials seen in HE neurons.

We further propose that this VJ bursting activity is what couples Ldv contractions to HT contractions. When VJ bursts occurred rarely, both Ldv and HT could spontaneously and independently contract (Fig. 5b), yet they appeared to be coupled when VJ bursts occurred (Fig. 5a). Our data suggest that the threshold for contraction of the AV is lower than that for the HT contraction. The number of AV contractions was greater than the number of HT contractions over the same time interval, suggesting a more

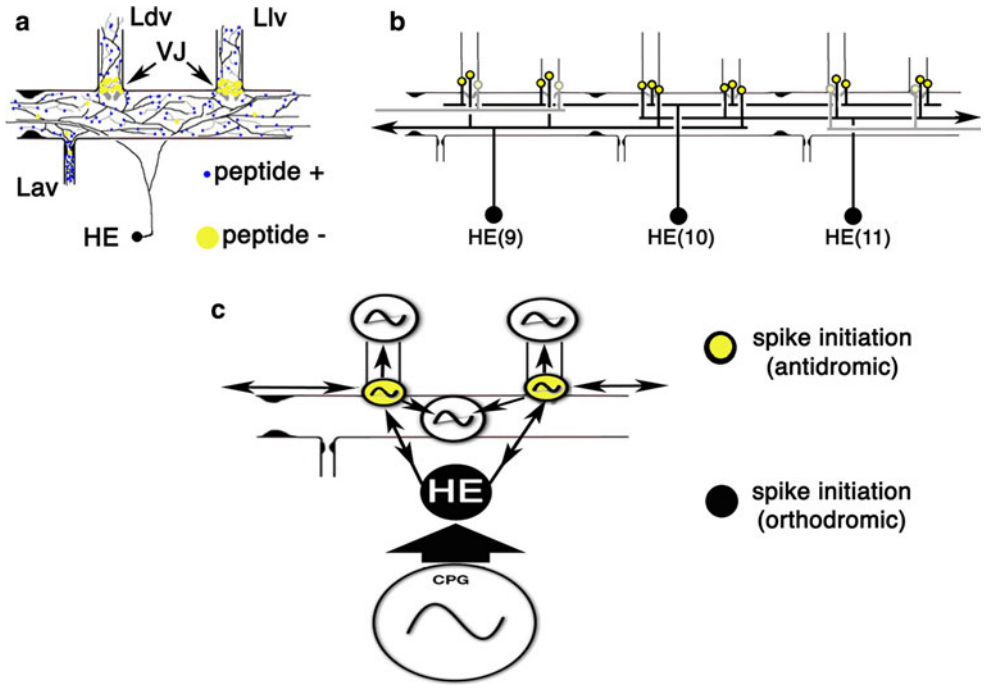

Fig. 11 Anatomical and physiological model of peripheral circuitry. **a** A model diagram of the location of HE varicosities along a single segmental HT module. Most varicosities contain peptide (*blue*) but some lack the peptide (*yellow*). A dense grouping of HE varicosities is present at the VJ regions. **b** Schematic representation of the observed overlap in intersegmental branches of HE axons in the midbody. **c** Schematic representation of proposed physiological model of coupled peripheral oscillators entrained by a CPG where the fastest oscillator (CPG) normally entrains the interconnected VJs (*yellow*). Segmental VJs are linked by coupling intersegmentally and VJ activity links myogenic oscillators on Ldv and Llv with HT. *Arrows* denote proposed pathways for possible action potential conduction as revealed by the experiments reported here

spontaneous endogenous oscillator in AVs. Furthermore, there was an occasional appearance of rapid doublet contractions in AV not usually seen in HT. In our model, we propose that the rapid entrainment of the VJ region by convergent focal HE innervation triggers the contractions of AV and HT such that there is a small but reliable phase lead in the AVs.

In addition to the focal innervation of strategically located VJ regions, the model also incorporates observations that HE innervation is intersegmental (Fig. 11b), which is established during early embryogenesis (see Figs. 2, 3 and 4 in Jellies et al. 1992) and retained in older animals (Kueh and Jellies 2012). We currently do not know the degree of variability associated with innervation or whether the intersegmental axons are symmetrical in both directions. There is significant metameric condensation of the anterior and posterior ends of the animal during development (Jellies et al. 1996), and the extent of innervation is determined by timing and target contact (Jellies 1995; Jellies and Kopp 1995; Harik et al. 1999) by axons belonging to HE neurons extending over three or more segments. In this light, it is interesting to note that previous studies on intersegmental phase of HT contraction have documented a distinction between phasing in the midbody when compared to the ends of the animal (Wenning et al. 2004a).

It has been established that there is central pattern generator entrainment of HE neurons, which then generate action potentials that entrain HT (Thompson and Stent 1976a, b, c; Maranto and Calabrese 1984a). Likewise, it is known that the circular muscle of the HT and side vessels exhibits myogenic activity (Thompson and Stent 1976a; Calabrese and Maranto 1984; Maranto and Calabrese 1984b) and that there is electrical coupling between HT muscle cells (Maranto and Calabrese 1984b). This suggests that there are myogenic oscillators and our work supports this (Fig. 5b). More specifically, we now add the specialized VJ regions, strategically located peripheral oscillators entrained by HE neurons and coupled in the periphery. The evidence that these VJ regions are oscillators comes primarily from the bursts obtained and responses during sequential elimination of orthodromic entrainment (Figs. 2, 3, 5, 8, 9, 10). Absent central pattern generator entrainment the VJ region produces a very long burst (3- 5 s) of action potentials, with variable period averaging about 1.5 cycles/minute (Figs. 2, 4, 5b). Further support for our suggestion that VJ regions are peripheral oscillators and that they are sources of antidromic action potentials derives from nerve cut and cell hyperpolarization experiments while recording intracellularly from HE neurons. Figure 11c summarizes the functional connectivity amongst oscillators of the peripheral network.

When we eliminated orthodromic input by hyperpolarizing the HE neuron centrally, we found that HE activity mirrored that seen in the VJ under comparable conditions (Figs. 8, 9). We also observed that the antidromic action potentials arrived at the HE soma centrally with little delay (Figs. 8c, 9b). This suggests that the activity originated at the VJ region, which had initiated a HT contraction with an expected latency of about 1.5 s (Fig. 6), yet observed centrally it was conducted at some velocity back toward the central nervous system, arriving after 1–2 s as a mere reporting of what had already occurred in the periphery. We have also recorded from the VJ and the cut anterior nerve near the central nervous system and have recorded action potentials arising first at VJ and being conducted antidromically (Fig. 9d, e). The antidromic activity revealed in this procedure is indistinguishable from what was originally described by Thompson and Stent (1976a) as an "afferent burst." Thompson and Stent (1976a) determined that the antidromic burst was conveyed by axons belonging to HE neurons, and our results show that it is associated with the VJ region in the periphery.

Peripheral neurogenic rhythm and oscillators

Thompson and Stent (1976a) first noted unexplained antidromic action potentials coursing from one segment to another in the vascular nerve. In extending those observations, Calabrese and Maranto (1984) and Maranto and Calabrese (1984b) obtained antidromic activity by hyperpolarizing an HE soma in the central nervous system under various conditions of surgical reduction of the periphery. Since spontaneous antidromic bursts were obtained in preparations where the HE neuron soma had been severed from its terminals, they termed this activity a "peripheral neurogenic rhythm." However, almost all subsequent data were recorded with the HE and HT connected, and with various lengths of HT. In our experiments, when there was only one HE neuron innervating the HT, which was silenced by hyperpolarization, we obtained a unique and previously undescribed behavior, long antidromic bursts that resembled long VJ bursts. We suggest that these long peripheral VJ bursts represent the basic peripheral network oscillator with HT intact as represented in Fig. 11c, and that it can be active without entrainment. Interestingly, Thompson and Stent (1976a) suggested that there would be peripheral oscillation, and Maranto and Calabrese (1984b) suggested that there might be some sort of coupled peripheral interactions between HE neurons. Our present results support both such interactions and suggest that they are involved in entraining the HT.

Intersegmental coupling

Our results strongly support the existence of peripheral intersegmental coupling among HE neurons. In contrast to

the long bursts seen when all nerves were transected, a different behavior was generated when we silenced HE(M10) by hyperpolarization while innervation from adjacent HE neurons in M9 and M11 remained intact (Fig. 8d). In our studies, the inferred central pattern generator frequency was not different from the antidromic burst frequency (Fig. 9a). We suggest that this activity does not represent a peripheral neurogenic oscillator. Rather, we suggest that these bursts (Fig. 8d) were being entrained by the central pattern generator through the HE neuron from M9 to 11 that projected their axons to the VJ regions and that the antidromic activity recorded in HE(M10) was simply the result of this entrainment seen through peripheral coupling of HE activity. Several observations support this suggestion. First, the burst durations of this antidromic activity were comparable to those for VJ bursts entrained by orthodromic activity (Figs. 4, 9c). Second, the latency between the burst and the HT contraction was much longer than that seen in the long spontaneous peripheral burst (Fig. 9b). Indeed, the latency was intermediate between the control (9, 10, 11) condition and "all cut" condition mimicked by our procedure. Since the conduction paths from the ganglion to the HT are the same for all three adjacent HE neurons, that portion of conduction delay would be equal. We suggest the intermediate delay involved would be that between VJ regions, a shorter distance. Finally, antidromic action potentials occurring at the CPG frequency could be recorded from a cut nerve as long as the two adjacent HE neuron pathways were intact (Fig. 9d). The mechanism of peripheral intersegmental coupling of activity can be examined in the future by simultaneously recording intracellularly from the HE and extracellularly from multiple adjacent VJs in the periphery. This would allow for the intra- and extracellular burst structures to be compared in detail, and also allow for experimental stimulation to insert bursts to see if rhythms can be reset or changed, something we were unable to do in the present studies.

Specialized innervated peripheral oscillators

An observation was also made by Kuhlman et al. (1985b) that we found intriguing in light of our present physiological study (Fig. 11) and the previous anatomical study that HE terminals in VJ regions appear to be deficient in peptide (Kueh and Jellies 2012). In examining the influence of the peptide FMRFamide on the heart system, Kuhlman et al. (1985b) bath applied FMRFamide while recording the antidromic bursts previously described as a peripheral neurogenic rhythm (Fig. 4 in Kuhlman et al. 1985b). They found that the peptide obliterated the antidromic activity in the HE neuron. It seems that the peptide negates the initiation of HE action potentials at the peripheral sites, where the antidromic action potentials are initiated. Since we suggest that the innervated VJ regions are sources of these action potentials, it is worth emphasizing that the HE terminals at VJ regions specifically exclude the peptide (Fig. 11 and Kueh and Jellies 2012). Based on the staining of acetylcholinesterase in our previous anatomical study as well as the presence of presynaptic terminals that contained primarily clear vesicles in the VJs as shown by Hammersen et al. (1976), these peptide-negative terminals have been inferred to be primarily cholinergic (Kueh and Jellies 2012). The release of acetylcholine alone might be sufficient to generate rapid phasic responses leading to the VJ bursts we describe that would be compromised if peptide were released in these locations. Focal application of the peptide and acetylcholine antagonists in future experiments may allow us to test the predicted effects on VJ activity.

The results of our present study strongly suggest that an isolated HE neuron is not a final common pathway for centrally generated activity. Instead, we put forward that the peripheral pattern of intersegmental innervation combined with interactions of multiple peripheral oscillators plays an active role in generating the robust coordinated behavior that characterizes this system. The model presented suggests that further studies will extend our understanding of how central and peripheral neural circuits contribute to generating fully functional and adaptive behaviors.

Acknowledgments This work was funded in part by a Faculty Research and Creative Activities Award from Western Michigan University (J.J.) and a National Science Foundation REU award # DBI-1062883. We gratefully acknowledge the assistance of Michelle Alfert in helping gather and analyze preliminary data in intact animals and Wesley J. Thompson for his thoughtful insights on the data reported in this manuscript.

References

Arbas EA, Calabrese RL (1990) Leydig neuron activity modulates heartbeat in the medicinal leech. J Comp Physiol A 167:665–671

Brezina V, Orekhova IV, Weiss KR (2000) The neuromuscular transform: the dynamic, nonlinear link between motor neuron firing patterns and muscle contraction in rhythmic behaviors. J Neurophysiol 83:207–231

Calabrese RL, Maranto AR (1984) Neural control of the hearts in the leech, *Hirudo medicinalis*. III. Regulation of myogenicity and muscle tension by heart accessory neurons. J Comp Physiol A 154:393–406

Calabrese RL, Maranto AR (1986) Cholinergic action on the heart of the leech, *Hirudo medicinalis*. J Exp Biol 125:205–224

Calabrese RL, Norris BJ, Wenning A, Wright TM (2011) Coping with variability in small neuronal networks. Integr Comp Biol. doi: 10.1093/icb/icr074

Cang J, Friesen WO (2000) Sensory modification of leech swimming: rhythmic activity of ventral stretch receptors can change intersegmental phase relationships. J Neurosci 20:7822–7829

Cang J, Friesen WO (2002) Model for intersegmental coordination of leech swimming: central and sensory mechanisms. J Neurophysiol 87:2760–2769

Chen J, Iwasaki T, Friesen WO (2011) Mechanisms underlying rhythmic locomotion: dynamics of muscle activation. J Exp Biol 214:1955–1964

Cohen AH, Wallen P (1980) The neuronal correlate of locomotion in fish: "fictive swimming" induced in an in vitro preparation of the lamprey spinal cord. Exp Brain Res 41:11–18

Delcomyn F (1980) Neural basis of rhythmic behavior in animals. Science 210:492–498

Deller SRT, MacMillan DL (1989) Entrainment of the swimmeret rhythm of the crayfish to controlled movements of some of the appendages. J Exp Biol 144:257–278

Dickinson PS, Nagy F, Moulins M (1988) Control of central pattern generators by an identified neurone in crustacean: activation of the gastric mill motor pattern by a neurone known to modulate the pyloric network. J Exp Biol 136:53–87

Garcia PS, Wright TM, Cunningham IR, Calabrese RL (2008) Using a model to assess the role of the spatiotemporal pattern of inhibitory input and intrasegmental electrical coupling in the intersegmental and side-to-side coordination of motor neurons by the leech heartbeat central pattern generator. J Neurophysiol 100:1354–1371

Goaillard JM, Taylor AL, Schulz DJ, Marder E (2009) Functional consequences of animal-to-animal variation in circuit parameters. Nat Neurosci 12:1424–1430

Grillner S, Parker D, Manira AE (1998) Vertebrate locomotion—a lamprey perspective. NY Acad Sci 860:1–18

Hammersen F, Staudte H-W, Möhring E (1976) Studies of the fine structure of invertebrate blood vessels. II. The valves of the lateral sinus of the leech *Hirudo medicinalis* L. Cell Tissue Res 172:405–423

Harik TM, Attaman J, Crowley A, Jellies J (1999) Developmentally regulated target-associated cues influence axon sprouting and outgrowth and may contribute to target specificity. Dev Biol 212:351–365

Heitler WJ (1986) Aspects of sensory integration in the crayfish swimmeret system. J Exp Biol 120:387–402

Hildebrandt JP (1988) Circulation in the leech, *Hirudo medicinalis* L. J Exp Biol 134:235–246

Hughes GM, Wiersma CAG (1960) The co-ordination of swimmeret movements in the crayfish, *Procambarus clarkii* (Girard). J Exp Biol 37:656–672

Ikeda K, Wiersma CAG (1964) Autogenic rhythmicity in the abdominal ganglia of the crayfish: the control of swimmeret movements. Comp Biochem Physiol 12:107–115

Jellies JA (1995) Cellular interactions in the development of Annelid neuromuscular systems. Am Zool 35:529–541

Jellies J, Kopp DM (1995) Sprouting and connectivity of embryonic leech heart excitor (HE) motor neurons in the absence of their peripheral target. Invert Neurosci 1:145–157

Jellies J, Kopp DM, Bledsoe JW (1992) Development of segment- and target-related neuronal identity in the medicinal leech. J Exp Biol 170:71–92

Jellies J, Kopp DM, Johansen K, Johansen J (1996) Initial formation and secondary condensation of nerve pathways in the medicinal leech. J Comp Neurol 373:1–10

Kiehn O, Butt SJB (2003) Physiological, anatomical and genetic identification of CPG neurons in the developing mammalian spinal cord. Prog Neurobiol 70:347–361

Krahl B, Zerbst-Boroffka I (1983) Blood pressure in the leech *Hirudo medicinalis*. J Exp Biol 107:163–168

Kristan WB, Calabrese RL (1976) Rhythmic swimming activity in neurons of the isolated nerve cord of the leech. J Exp Biol 65:643–668

Kueh D, Jellies JA (2012) Targeting of a neuropeptide to discrete regions of the motor arborizations of a single neuron. J Exp Biol (in press)

Kuhlman JR, Li C, Calabrese RL (1985a) FMRF-amide-like substances in the leech. I. Immunocytochemical localization. J Neurosci 5:2301–2309

Kuhlman JR, Li C, Calabrese RL (1985b) FMRF-amide-like substances in the leech. II. Bioactivity on the heartbeat system. J Neurosci 5:2310–2317

Li C, Calabrese RL (1987) FMRF-amide-like substances in the leech. III. Biochemical characterization and physiological effects. J Neurosci 7:595–603

Lund JP (2011) Chew before you swallow. In: Gossard JP, Dubuc R, Kolta A (eds) Progress in brain research. Breathe, walk and chew the neural challenge: Part II. Elsevier, Amsterdam, pp 219–251

Maranto AR, Calabrese RL (1984a) Neural control of the hearts in the leech *Hirudo medicinalis.* I. Anatomy, electrical coupling, and innervation of the hearts. J Comp Physiol A 154:367–380

Maranto AR, Calabrese RL (1984b) Neural control of the hearts in the leech, *Hirudo medicinalis.* II. Myogenic activity and its control by heart motor neurons. J Comp Physiol A 154:381–391

Marder E, Calabrese RL (1996) Principles of rhythmic motor pattern generation. Physiol Rev 76:687–717

Marzullo TC, Gage GJ (2012) The SpikerBox: a low cost, open-source bioamplifier for increasing public participation in neuroscience inquiry. PLoS ONE 7:e30837

Morgan PT, Perrins R, Lloyd PE, Weiss KR (2000) Intrinsic and extrinsic modulation of a single central pattern generating circuit. J Neurophysiol 84:1186–1193

Muller KJ, Nicholls JG, Stent GS (eds) (1981) Neurobiology of the leech. Cold Spring Harbor, NY

Norris BJ, Weaver AL, Morris LG, Wenning A, Garcia PA, Calabrese RL (2006) A central pattern generator producing alternative outputs: temporal pattern of premotor activity. J Neurophysiol 96:309–326

Norris BJ, Weaver AL, Wenning A, Garcia PS, Calabrese RL (2007a) A central pattern generator producing alternative outputs: pattern, strength, and dynamics of premotor synaptic input to leech heart motor neurons. J Neurophysiol 98:2992–3005

Norris BJ, Weaver AL, Wenning A, Garcia PS, Calabrese RL (2007b) A central pattern generator producing alternative outputs: phase relations of leech heart motor neurons with respect to premotor synaptic input. J Neurophysiol 98:2983–2991

Norris BJ, Baquet G, Weaver AL, Morris LG, Wenning A, Garcia PA, Calabrese AL (2009) A central pattern generator producing alternative outputs: Temporal pattern of premotor activity. J Neurophysiol 96:309–326. doi:10.1152/jn.00011.2006

Norris BJ, Wenning A, Wright TM, Calabrese RL (2011) Constancy and variability in the output of a central pattern generator. J Neurosci 31:4663–4674

Nusbaum MP, Beenhakker MP (2002) A small systems approach to motor pattern generation. Nature 417:343–350

Pickard RS, Mill PJ (1974) Ventilatory movements of the abdomen and branchial apparatus in dragonfly larvae (Odonata: Anisoptera). J Zool 174:23–40

Rybak IA, Shevtsova NA, Lafreniere-Roula M, McCrea DA (2006) Modelling spinal circuitry involved in locomotor pattern generation: insights from deletions during fictive locomotion. J Physiol 577(2):617–639

Saideman SR, Blitz DM, Nusbaum MP (2007) Convergent motor patterns from divergent circuits. J Neurosci 27:6664–6674

Siddall ME, Tronrelj P, Utevsky SY, Nkamany M, Macdonald KS III (2007) Diverse molecular data demonstrate that commercially available medicinal leeches are not all *Hirudo medicinalis*. Proc Roy Soc B. doi:10.1098/rspb.2007.0248

Smarandache C, Hall WM, Mulloney B (2009) Coordination of rhythmic activity by gradients of synaptic strength in a neural circuit that couples modular neural oscillators. J Neurosci 29:9351–9360

Stein PSG, Grillner S, Selverston AI, Stuart DG (1997) Neurons, networks, and behavior. MIT Press, Cambridge

Stent GS, Kristan WB, Friesen WO, Ort CA, Poon M, Calabrese RL (1978) Neuronal generation of the leech swimming movement. Science 200:1348–1357

Thirumalai V, Marder E (2002) Colocalized neuropeptides activate a central pattern generator by acting on different circuit targets. J Neurosci 22:1874–1882

Thompson WJ, Stent GS (1976a) Neuronal control of heartbeat in the medicinal leech. I. Generation of the vascular constriction rhythm by heart motor neurons. J Comp Physiol 111:261–279

Thompson WJ, Stent GS (1976b) Neuronal control of heartbeat in the medicinal leech. II. Intersegmental coordination of heart motor neuron activity by heart interneurons. J Comp Physiol 111:281–307

Thompson WJ, Stent GS (1976c) Neuronal control of heartbeat in the medicinal leech. III. Synaptic relations of the heart interneurons. J Comp Physiol 111:309–333

Wagenaar DA, Hamilton MS, Huang T, Kristan WB, French KA (2010) A hormone-activated central pattern generator for courtship. Curr Biol 20:487–495

Weeks JC (1981) Neuronal basis of leech swimming: separation of swim initiation, pattern generation, and intersegmental coordination by selective lesion. J Neurophysiol 45:698–723

Wenning A, Meyer EP (2007) Hemodynamics in the leech: blood flow in two hearts switching between two constriction patterns. J Exp Biol 210:2627–2636

Wenning A, Cymbalyuk GS, Calabrese RL (2004a) Heartbeat control in leeches. I. Constriction pattern and neural modulation of blood pressure in intact animals. J Neurophysiol 91:382–396

Wenning A, Hill AAV, Calabrese RL (2004b) Heartbeat control in leeches. II. Fictive motor pattern. J Neurophysiol 91:397–409